Original Research

Novel small-molecule compound VCP979 attenuates renal fibrosis in male rats with unilateral ureteral obstruction

Shudan Min[1], Di Chang[1], Yuan-Cheng Wang[1], Ting-Ting Xu[1], Hong Ge[1], Jilei Zhang[2], Binghui Wang[3,4] and Shenghong Ju[1]

[1]Jiangsu Key Laboratory of Molecular and Functional Imaging, Department of Radiology, Zhongda Hospital, Medical School of Southeast University, Nanjing 210009, China; [2]Clinical Science, Philips Healthcare, Shanghai 200072, China; [3]Biomarker Discovery Laboratory, Baker Heart and Diabetes Institute, Melbourne, VIC 3004, Australia; [4]Monash Centre of Cardiovascular Research and Education in Therapeutics, Department of Epidemiology and Preventive Medicine, Monash University, Melbourne VIC 3004, Australia

Corresponding author: Shenghong Ju. Email: jsh0836@hotmail.com

Impact Statement

Renal fibrosis is a hallmark of chronic kidney disease, while efficient therapy against renal fibrosis is still lacking. Here, we investigated a potential role of a novel small-molecule compound VCP979 in renal fibrosis in a rat model of unilateral ureteral obstruction, and demonstrated that treatment with VCP979 ameliorated renal function and pathological renal fibrosis via its antifibrotic and anti-inflammatory effects. Further study of T1rho mapping displayed decreased T1rho values after VCP979 treatment with a linear correlation between the T1rho values and the fibrosis, indicating that T1rho mapping is a non-invasive imaging strategy to detect the alteration of renal fibrosis. These results indicated that VCP979 may serve as a small-molecule drug for preventing the progression of renal fibrosis, which might help in developing novel small-molecule agents for ameliorating clinical renal fibrosis and meanwhile facilitating the real-time evaluation of therapeutic efficacy of these drugs *in vivo*.

Abstract

Renal fibrosis is a hallmark of chronic kidney disease, while efficient therapy against renal fibrosis is still lacking. In this study, we investigated the role of a novel small-molecule compound VCP979 on renal fibrosis and inflammation in a rat model of unilateral ureteral obstruction (UUO). One week after the UUO surgery, rats were administered VCP979 by gavage for one week, and after treatment, magnetic resonance imaging of T1rho mapping and histopathological analysis were performed to evaluate renal fibrosis *in vivo* and *ex vivo*. This study showed that treatment with VCP979 effectively reduced renal fibrosis, extracellular matrix accumulation, and alleviated epithelial–mesenchymal transition in UUO rats, as well as improved renal function. *In vivo* T1rho mapping displayed increased T1rho values in the UUO rats, which was decreased after VCP979 treatment, and a positive correlation was detected between the T1rho values and the percentage of fibrotic area. Moreover, the administration of VCP979 also ameliorated the inflammatory cytokines expression and the infiltration of macrophages in renal tissues. Mechanistically, VCP979 treatment inhibited the activation of p38 mitogen–activated protein kinase, nuclear factor-kappa B, and transforming growth factor-β1/Smads signaling pathways. These results indicated that VCP979 could be an effective therapeutic agent for alleviating renal fibrosis and inflammation in the rat model of UUO via its antifibrotic and anti-inflammatory effects.

Keywords: Renal fibrosis, VCP979, p38 MAPK, MRI, T1rho mapping, inflammation

***Experimental Biology and Medicine* 2023; 248: 327–338. DOI: 10.1177/15353702221147569**

Introduction

Renal fibrosis is a pathological hallmark of chronic renal disease, and represents the common pathway of end-stage renal failure.[1,2] However, efficient therapy against renal fibrosis is still lacking. Accumulating data implicate that renal fibrotic process is involved in tubulointerstitial damage, inflammatory cells recruitment, and extracellular matrix (ECM) deposition, which is closely correlated to loss of renal function.[3] Therefore, it is urgent to develop effective drugs against renal fibrosis. Considerable evidence verifies that small-molecule compounds with a low molecular weight display high-affinity binding *in vivo* and are easier to absorb than protein-based drugs in various diseases.[4] Thus, small-molecule drugs may contribute to the development of novel therapeutic for the inflammatory-fibrotic process in renal fibrosis.

The p38 mitogen-activated protein kinase (MAPK) pathway is an essential intracellular signal transducer responding to cellular stimuli including a variety of inflammatory/fibrotic cytokines.[5,6] It elicits diverse pro-inflammatory and pro-fibrotic effects and is related to various cellular

disorders in kidney diseases, such as glomerulosclerosis in diabetic nephropathy,[7] renal atrophy, and renal artery stenosis.[8] Previous studies have shown that the p38 MAPK involves in a direct transforming growth factor-β (TGF-β) signaling pathway to facilitate fibrogenesis, and blockade of p38 MAPK relieves tissue fibrosis in different animal models.[9–11] However, the commonly used p38 MAPK inhibitor SB203580 showed a poor potency and high toxicity due to the interference with other protein kinases.[12] Recently, we have developed a novel small-molecule compound VCP979 as a selective inhibitor of p38 MAPK, which presents a good affinity and inhibitory activity for the p38 MAPK.[13,14] Our previous study has demonstrated the role of VCP979 in promoting axonal/white matter remodeling and ischemic stroke recovery in type 2 diabetic mice, which is accomplished by attenuating the inflammatory gene expression and reducing the activation of p38 MAPK/nuclear factor-kappa B (NF-κB) pathways.[15] However, the effect of VCP979 on unilateral ureteral obstruction (UUO)-induced renal fibrosis has not been investigated.

Although percutaneous renal biopsy is widely adopted as the reference standard method to measure renal fibrosis,[16] it is invasive and sampled tissues may be unrepresentative for assessing renal fibrosis.[17,18] Thus, there is a need to establish an accurate and non-invasive method for measuring the effect of VCP979 treatment on renal fibrosis. Magnetic resonance imaging (MRI) may provide valuable information, and T1rho mapping is an endogenous contrast imaging method to characterize tissue without gadolinium-based contrast agents.[19] T1rho mapping reflects the interactions between motion-restricted water molecules and local macromolecular environment;[20] hence, it is utilized to study macromolecular composition and proton due to its sensitivity to low-frequency motional and static processes.[21] Recently, T1rho mapping has been applied to detect liver fibrosis,[22] diffuse myocardial fibrosis,[23] and renal allograft fibrosis,[24,25] suggesting that T1rho mapping is a non-invasive diagnostic tool for fibrosis detection.

The aim of this study was to explore the therapeutic efficacy of a small-molecule compound VCP979 on renal fibrosis in a rat model of UUO, and T1rho mapping was utilized to detect the alteration of renal fibrosis after VCP979 treatment non-invasively. These results may provide valuable evidences into the application of novel small-molecule agents in murine models of renal fibrosis.

Materials and Methods

Animal experiments

All experimental protocols were approved by the Institutional Animal Use and Care Committee of Southeast University, Nanjing, China (SYXK-20180315004). This study was carried out in compliance with the Animal Research: Reporting of In Vivo Experiments (ARRIVE) guidelines.[26] VCP979 was developed and provided by Binghui Wang at Monash University, Australia. Eight-week-old male Wister rats were purchased (Yangzhou University Animal Center, China), and all rats were maintained in standard animal facilities at 22–26°C and 40–70% humidity on a cycle of 12 h light–dark cycle with food and water available *ad libitum*. After adaptive feeding for one week, these rats were randomly divided into three groups. A model of UUO was performed in Wistar rats, which was induced by an incision from the back, and the left ureter was exposed and ligated near the renal pelvis as described previously.[27] A group of sham-operated rats (Sham, $n = 8$) was used as the control. Those rats were incised from the back, and the left ureter was exposed without ligation. One week after surgery, rats were randomized to receive either an oral administration of vehicle (0.5% methyl cellulose, twice a day; UUO + Veh, $n = 8$) or an oral administration of VCP979 dissolved in methyl cellulose (50 mg/kg, twice a day; UUO + VCP979, $n = 8$) for one week. Blood and urine were collected one and two weeks after the surgery, and serum creatinine (SCr), blood urea nitrogen (BUN), and urinary protein were acquired to evaluate renal function. Moreover, levels of alanine aminotransferase (AST) and aspartate aminotransferase (ALT) in the serum of animal models were acquired to evaluate the toxicity of VCP797. The body weights of rats were assessed once per three days. Two weeks after surgery, rats were scanned with MRI, and after that, all rats were sacrificed with tissues harvested. Pentobarbital was used for anesthesia and euthanasia.

Renal function analysis

Twenty-four hours urine samples were collected by metabolic cages, and the volumes of urine were recorded. Blood samples of rats were obtained from the angular vein two weeks after surgery in all rats. Plasma was acquired from the serum of the samples through centrifugation, and anticoagulant (ethylenediaminetetraacetic acid, EDTA) was added in the tubes before collection. Levels of SCr, BUN, and 24 h urine protein were determined on a clinical chemistry analyzer (AU5821, Beckman Coulter, Bera, CA, USA) in Zhongda Hospital.

Phantom study of MRI

Experiments were performed on phantoms at first to examine the accuracy and repeatability of the T1rho mapping sequence, and magnetic resonance (MR) scans were performed with a 3.0 T clinical scanner (Ingenia 3.0 T, Philips Healthcare, Amsterdam, The Netherlands) with a 16-channel animal coil (Chenguang, Shanghai, China). Four phantom tubes were created in 15 mL centrifugal tube (15 mm diameter) by dissolving agarose powder in deionized water at different concentrations (weight/volume, 1%, 2%, 3%, and 4%), and phantom tubes were placed in a bottle filled with deionized water. Then, the phantom tubes were scanned, and the T1rho mapping images were acquired using a turbo field echo (TFE) sequence with stretched adiabatic as the spin-lock pulse type. Table 1 shows parameters of T2-weighted imaging (T2WI) sequence and T1rho mapping sequence. To calculate the T1rho values, regions of interest (ROIs) were drawn manually over the phantom tubes. As for ROI selection, a circular ROI sized 50 pixels was chosen in the center of the T1rho map of each phantom. The T1rho maps were calculated with four different time of spin-locks (TSLs) based on monoexponential decay model using pixel-by-pixel methods, which can be presented by the following equation

Table 1. Parameters of MR scanning.

Parameters	T2-weighted imaging	T1rho mapping
Fast imaging mode	TSE	TFE
Repetition time (ms)	1789	5.8
Echo time (ms)	93	2.8
Matrix	320 × 315	100 × 100
Orientation	Transverse	Transverse
Field of view (mm)	80 × 80	60 × 60
Section thickness (mm)	2	4
Number of sections	15	5
Flip angle (degrees)	90	40
Number of signals acquired	3	4
TSL (ms)	–	0, 10, 20, 40
Acquisition time	3 min 56 s	9 min 45 s

MR: magnetic resonance; TSE: turbo spin echo; TFE: turbo field echo; TSL: time of spin-lock.
T1rho mapping with four TSLs was conducted using a TFE sequence with stretched adiabatic as the spin-lock pulse type.

$$M_{TSL} = M_0 exp\left(-\frac{TSL}{T1rho}\right)$$

where M_{TSL} denotes the magnetization with a spin-lock time, M_0 is the magnetization with $TSL = 0$ ms, and TSL denotes the duration of the spin-lock time.

In vivo MRI of animal study

Two weeks after surgery, rats were scanned with MRI. MR scans were performed with the 3.0 T clinical scanner and 16-channel animal coil as described above. The rats were positioned in a prone, head-first position inside the animal coil. The rats were anesthetized with 3% pentobarbital sodium (2 mL/kg) for better stability and repeatability for imaging acquisition. Parameters of T2WI sequence and T1rho mapping sequence were also listed in Table 1. To calculate the T1rho values, ROIs were drawn manually over the renal parenchyma referencing the T2WI.[28] As for ROI selection, five ROIs were sized 20–40 pixels approximately, evading the vessels and renal sinus, and the T1rho maps were calculated using the same equation as shown above in the phantom study.

Histological and immunohistochemical analyses

Tissues were fixed with 4% formaldehyde for 48 h and then embedded with paraffin. Kidney sections (4 μm) were stained with periodic acid–Schiff (PAS; G1281, Solarbio, Beijing, China), Masson's trichrome (Masson; G1340, Solarbio), and Sirius red (ab150681, Abcam, Cambridge, UK) as previously described.[29] Immunohistochemical (IHC) staining was performed in renal tissues by antibodies including fibronectin (ab2413, Abcam), E-cadherin (14472, Cell Signaling Technology, Danvers, MA, USA), Vimentin (5741, Cell Signaling Technology), α-smooth muscle actin (α-SMA; ab124964, Abcam), and CD68 (ab125212, Abcam) to evaluate tissue ECM deposition and epithelial–mesenchymal transition (EMT). Liver was stained with hematoxylin and eosin (H&E) to evaluate the toxicity of VCP797. Images were taken on a microscope (OLYMPUS, Tokyo, Japan), and at least five randomly chosen fields of stained slides were evaluated by technicians who were blinded by treatment groups. Quantitative assessment was performed by Image-Pro Plus 6.0 (Media Cybernetics, Rockville, MD, USA).

Cell culture

The human kidney-2 (HK-2) cells were purchased from the American Type Culture Collection. The HK-2 cells were cultured in Dulbecco's modified Eagle's medium/F-12 nutrient mixture (DMEM/F-12, Gibco, Invitrogen, CA, USA), containing 10% fetal bovine serum (FBS, Gibco, Invitrogen), 100 U/mL penicillin, and 100 μg/mL streptomycin in a humidified incubator at 37°C with 5% CO_2. For induction of EMT, HK-2 cells were starved without serum for 12 h and subsequently treated with (dimethyl sulfoxide, DMSO; the Vehicle group) or TGF-β1 (Peprotech, Rocky Hill, NJ, USA) at a concentration of 10 ng/mL for 48 h as described previously.[30] Then, the cells were treated with different concentrations of VCP979 (0.1, 1 and 10 μM) for another 24 h. For cell treatment, VCP979 was dissolved in DMSO at different concentrations, and an equal volume of DMSO was added into the cell culture medium of the control and TGF-β1 group. The toxicity of VCP979 was indicated by cell counting kit-8 (CCK-8) *in vitro*. HK-2 cells were treated with VCP979 for 24 h at concentrations of 0, 0.1, 1, 2, 5, and 10 μM, and the cell viability was measured by CCK-8 assay.

Western blot

Frozen kidney tissues and HK-2 cells were lysed to extract total protein using modified radioimmunoprecipitation assay buffer (RIPA) buffer with protease and phosphatase inhibitors. Protein concentrations were determined by bicinchoninic acid (BCA) protein quantitation assay (Key Gene Biotech, Jiangsu, China), and the western blot analysis of fibronectin, E-cadherin, α-SMA, Vimentin, NF-κB, phosphorylated NF-κB (p-NF-κB), p38, phosphorylated p38 (p-p38), TGF-β1, Smad2, phosphorylated Smad2 (p-Smad2), Smad3, phosphorylated Smad3 (p-Smad3), and glyceraldehyde 3-phosphate dehydrogenase (GAPDH) was conducted as described previously with specific antibodies (Supplementary Table 1).[31] Signals were visualized with the high-signal chemiluminescent western blotting substrate (Tanon, Shanghai, China) by Chemiluminescence imaging system (Clinx Science Instruments Co., Shanghai, China), and quantified by Image J (National Institutes of Health, Bethesda, MD, USA).

Quantitative real-time polymerase chain reaction

Total RNA was extracted from renal tissues with TRIzol reagent (Thermo Fisher, Waltham, MA, USA) and quantified with NanoDrop ND-2000 spectrophotometer (Thermo Fisher). Total RNA was reversely transcribed into complementary DNA (cDNA) with the PrimeScript RT reagent kit. The mRNA levels of tumor necrosis factor-α (TNF-α), interleukin-6 (IL-6), and interleukin-1β (IL-1β) were detected by reverse transcription quantitative real-time polymerase chain reaction (RT-qPCR) with an SYBR Green Master Mix

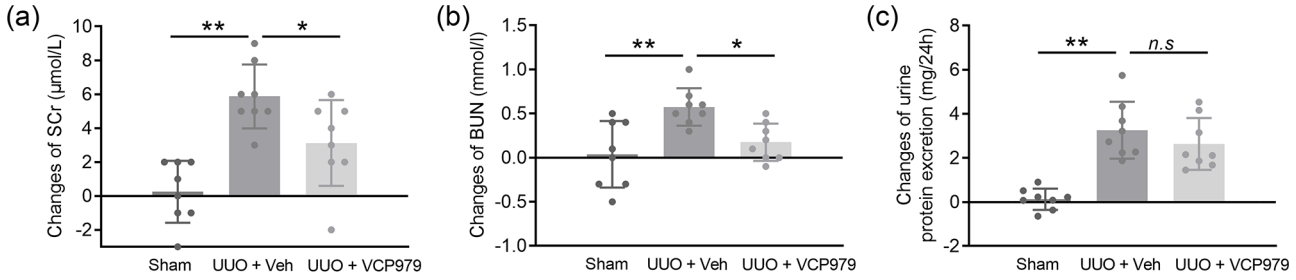

Figure 1. Effects of VCP979 on renal function in UUO-induced rats. (a) The changes of serum creatinine (SCr), (b) blood urea nitrogen (BUN), and (c) 24 h urine protein excretion in UUO-induced rats ($n = 8$ per group). All data were presented as mean ± SD.
*$P < 0.05$; **$P < 0.01$.

kit (Takara Bio, Shiga, Japan) with real-time polymerase chain reaction (PCR) systems (Thermo Fisher). The PCR procedure was set for 95°C for 30 s, 57°C for 30 s, and 30 s at 70°C. The level of mRNA expression was calculated with the $2^{-\Delta\Delta Cq}$ method, with the *GAPDH* genes as the control. The primer sets used to identify the gene are as follows:

GAPDH-F: 5′-TGCACCACCAACTGCTTAGC-3′;
GAPDH-R: 5′-GGCATGCACTGTGGTCATGAG-3′;
TNF-α-F: 5′-GCGACGTGGAACTGGCAGAAG-3′;
TNF-α-R: 5′-GCCACAAGCAGGAATGAGAAGAGG-3′;
IL-6-F: 5′-ACTTCCATCCAGTTGCCTTCTTGG-3′;
IL-6-R: 5′-TTAAGCCTCCGACTTGTGAAGAG-3′;
IL-1β-F: 5′-TCGCAGCAGCACATCAACAAGAG-3′;
IL-1β-R: 5′-TGCTCATGTCCTCATCCTGGAAGG-3′.

Statistical analysis

The normality assumption was assessed with the Shapiro–Wilk test. The significance of the differences in all data among the three groups was evaluated with either a one-way analysis of variance or, if normality was violated, a non-parametric Kruskal–Wallis test (specifically refer to the ratio of p-Smad3/Smad3 protein expression in western blot, the tubular injury score in PAS staining, the IHC staining of α-SMA and CD68 positive macrophages), followed by post hoc multiple comparisons with either the Bonferroni (equal variance assumed) or Dunn (unequal variance assumed) test. All statistical tests were performed with the GraphPad Prism version 8.0 (GraphPad Software, San Diego, CA, USA), and two-tailed $P < 0.05$ was considered as a statistically significant difference. Data are presented as the mean value ± SD.

Results

Effects of VCP979 administration on renal function in UUO rats

The changes of SCr and BUN between pre- and post-treatment were significantly increased in the UUO + Veh group compared with the Sham group ($P < 0.01$), which was significantly reduced in the UUO + VCP979 group compared with the UUO + Veh group ($P < 0.05$) after VCP treatment (Figure 1(a) and (b)). The change of 24 h urine protein excretion between pre- and post-treatment was also significantly increased in the UUO + Veh group compared with the Sham group ($P < 0.01$; Figure 1(c)). These results indicated improved renal function after VCP979 treatment in UUO rats. Detailed values of SCr, BUN, and 24 h urine protein excretion of the UUO rats were listed in the supplementary files (Supplementary Table 2 and Figure 1).

MRI validation in phantom study

The phantom images of T2WI (Figure 2(a)) and T1rho map (Figure 2(b)) with different T1rho relaxation times were scanned and reconstructed. As shown in Figure 2(c), T1rho values of phantoms varied with agarose concentration, and exhibited a linear correlation with concentration ($R^2 = 0.9242$; $P < 0.05$), which demonstrated that the T1rho mapping is sensitive to reflect the concentration of macromolecules in phantoms.

VCP979 alleviated renal fibrosis in UUO rats as assessed by pathological staining

Damaged integrity of renal tissues and evident dilatation of tubule were observed in the PAS staining (Figure 3(a)), and the tubular injury score was significantly increased in the UUO + Veh group compared with the Sham group ($P < 0.01$), which was decreased after VCP979 treatment ($P < 0.01$). Masson (Figure 3(b)) and Sirius red staining (Figure 3(c)) showed significantly increased renal fibrosis in the UUO + Veh group compared with the Sham group ($P < 0.01$), which was decreased after VCP979 treatment ($P < 0.01$). In addition, increased expression of fibronectin was detected in the UUO + Veh group compared with the Sham group ($P < 0.01$), while VCP979 treatment mitigated the expression of fibronectin in the UUO kidneys ($P < 0.01$; Figure 3(d)), demonstrating that VCP979 could attenuate renal ECM deposition in the UUO rat model.

VCP979 alleviated renal fibrosis in UUO rats as assessed by MRI

Gross pathology showed different macroscopic appearances of renal tissues in the three groups, which were enlarged in the UUO rats (Figure 4(a)). T2WI showed that compared with the Sham group, the renal pelvis was filled with accumulated urine with an enlarged shape and thin parenchyma in the UUO + Veh and UUO + VCP979 groups (Figure 4(b)). Interestingly, the UUO + Veh group exhibited significantly increased T1rho values compared with the Sham group

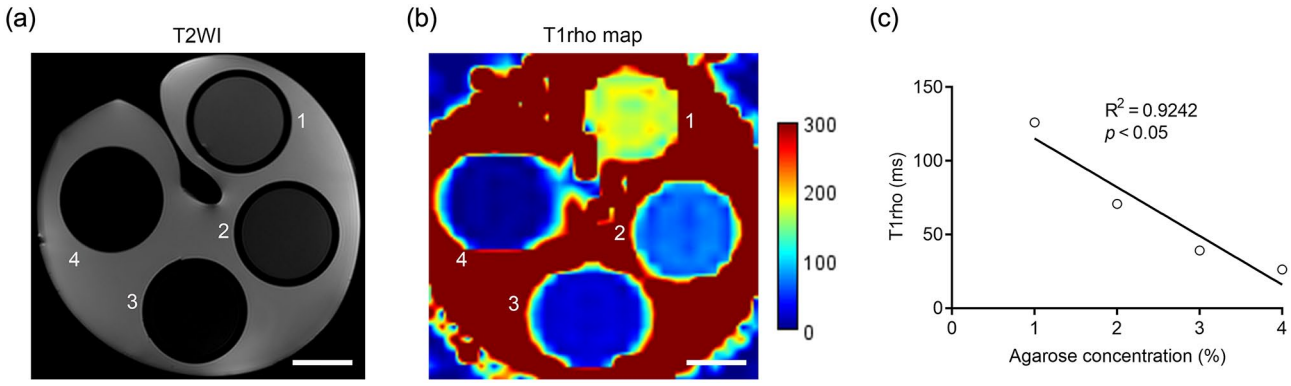

Figure 2. Magnetic resonance imaging of phantoms. (a) T2-weighted images and (b) T1rho maps of agarose phantoms (scale bars = 1 cm). (c) The correlation between mean T1rho values and the concentrations of agarose phantoms.

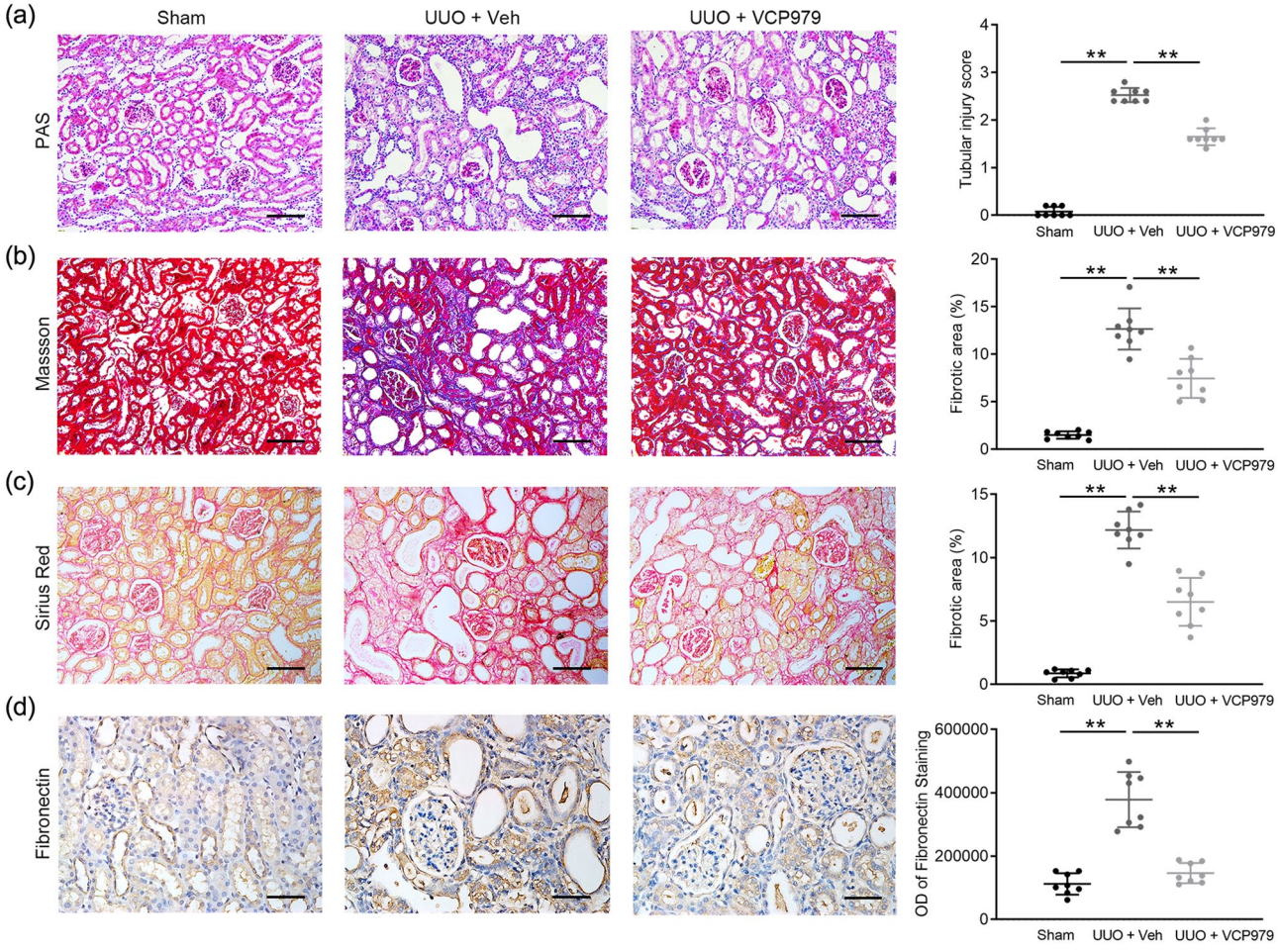

Figure 3. VCP979 attenuated renal fibrosis in UUO rats. (a) Representative images of periodic acid–Schiff (PAS) staining of kidney tissues in rats from three groups and measured tubular injury score ($n = 8$ per group; scale bars = 100 μm). (b) Masson staining of kidney tissue in rats from three groups and measured percentage of fibrotic areas ($n = 8$ per group; scale bars = 100 μm). (c) Sirius red staining of kidney tissue in rats from three groups and measured percentage of fibrotic areas ($n = 8$ per group; scale bars = 100 μm). (d) Immunochemical staining of fibronectin in kidney tissue of rats and measured optical density (OD) values of fibronectin positive areas ($n = 8$ per group; scale bars = 50 μm). All data were presented as mean ± SD.
*$P < 0.05$; **$P < 0.01$.

($P < 0.01$), which was decreased after VCP979 treatment ($P < 0.05$; Figure 4(c) and (d)), demonstrating that T1rho MRI was capable to detect the alteration of renal tissue fibrosis non-invasively. Furthermore, there is a positive correlation between the T1rho values and the percentage of fibrotic area as measured by the Masson staining ($R^2 = 0.808$; $P < 0.001$; Figure 4(e)) and Sirius red staining ($R^2 = 0.886$; $P < 0.001$; Figure 4(f)), which indicated the feasibility of applying T1rho

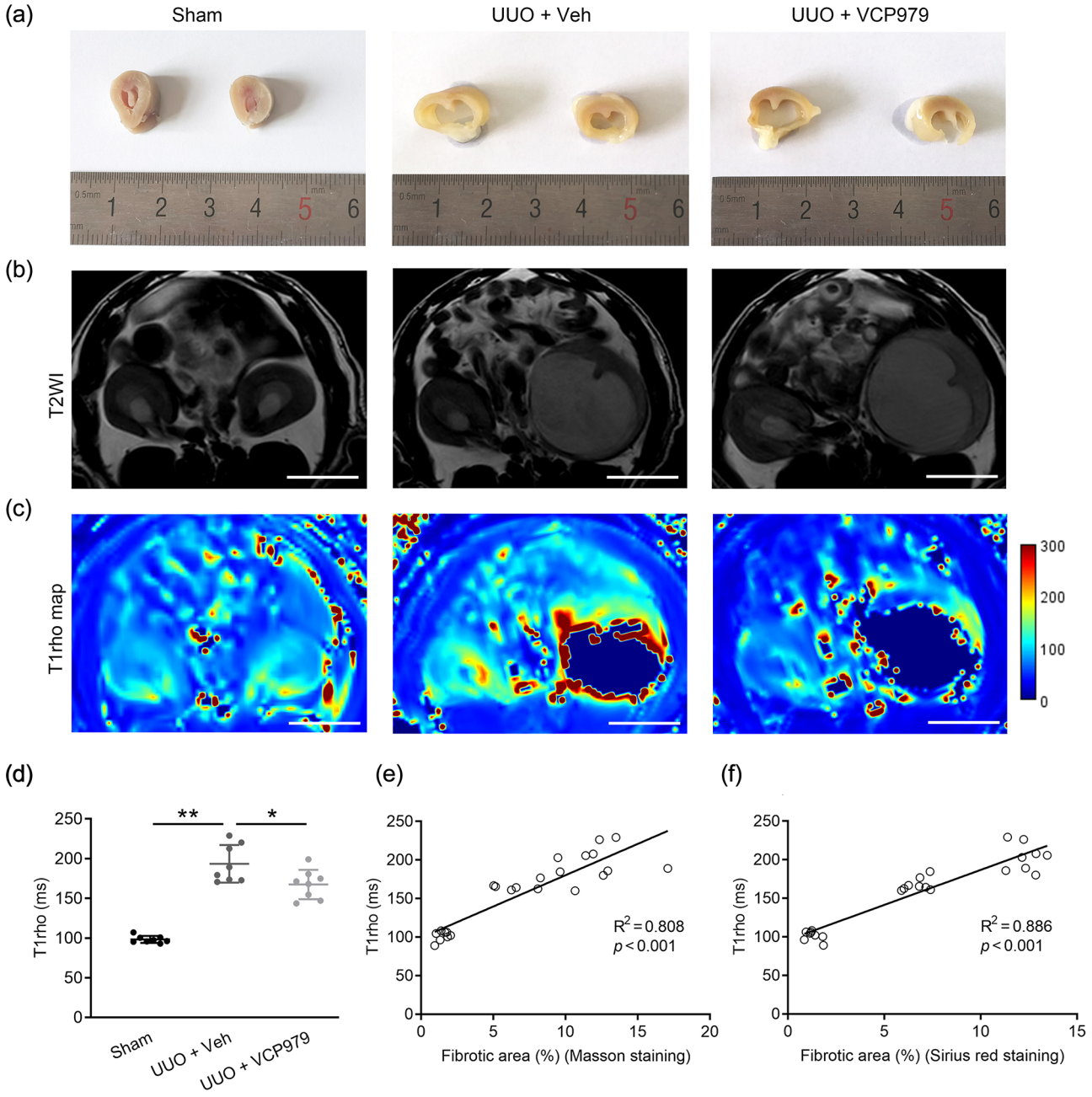

Figure 4. Magnetic resonance imaging of renal fibrosis in UUO rats. (a) Gross pathology of renal tissues from the three groups. (b) T2-weighted images (T2WI) of rats (scale bars = 1 cm). (c) T1rho maps and (d) measured T1rho values of rats ($n = 8$ per group; scale bars = 1 cm). (e) Linear correlations between T1rho values and percentage of fibrotic area in the Masson staining and (f) Sirius red staining ($n = 8$ per group). All data were presented as mean ± SD.
*$P < 0.05$; **$P < 0.01$.

MRI to quantify the alterations of renal fibrosis in UUO rats *in vivo*.

VCP979 alleviated EMT in UUO rats and TGF-β1-induced HK-2 cells

The effect of VCP979 on EMT in UUO rats was analyzed by measuring the expression of E-cadherin, α-SMA and Vimentin. IHC of E-cadherin, α-SMA and Vimentin (Figure 5(a)) revealed that compared with the UUO + Veh group, treatment with VCP979 significantly upregulated the level of E-cadherin ($P < 0.01$; Figure 5(b)), and downregulated the protein levels of α-SMA ($P < 0.05$; Figure 5(c)) and Vimentin ($P < 0.01$; Figure 5(d)) in UUO rats. In addition, the effects of VCP979 were further confirmed by the western blot analysis (Figure 5(e)), and the protein expression of E-cadherin (Figure 5(f)), α-SMA (Figure 5(g)), and Vimentin (Figure 5(h)) was significantly ameliorated after VCP979 treatment ($P < 0.01$). EMT in HK-2 cells was stimulated by TGF-β1, and the western blot (Figure 5(i)) revealed that

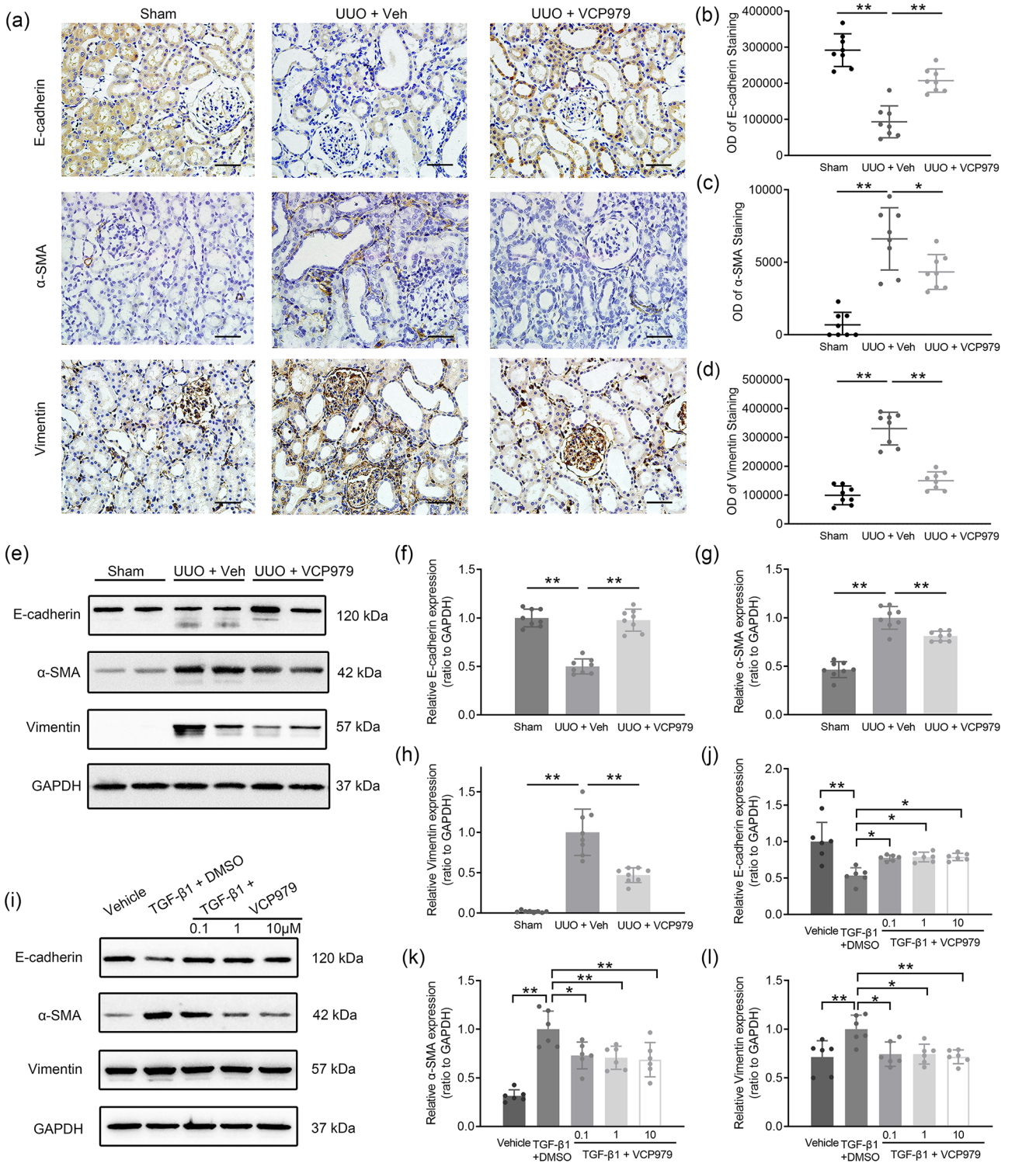

Figure 5. VCP979 alleviated epithelial–mesenchymal transition in UUO rats and TGF-β1-induced HK-2 cells. (a) Immunochemical staining and measured optical density (OD) values of E-cadherin (b), α-SMA (c), and Vimentin (d) in the kidney tissues of rats ($n = 8$ per group; scale bars = 50 μm). (e) Western blots analysis and measured protein expression of E-cadherin (f), α-SMA (g), and Vimentin (h) in the kidney tissue of rats ($n = 8$ per group). (i) Western blot analysis and measured protein expression of E-cadherin (j), α-SMA (k), and Vimentin (l) in TGF-β1-induced HK-2 cells ($n = 6$ per group). All data were presented as mean ± SD. $^{*}P < 0.05$; $^{**}P < 0.01$.

compared with the Vehicle group, TGF-β1 stimulation significantly reduced the expression of E-cadherin (Figure 5(j)) and increased the expression of α-SMA (Figure 5(k)) and Vimentin (Figure 5(l)) in HK-2 cells ($P < 0.05$), while VCP979 treatment significantly mitigated these alterations in HK-2 cells ($P < 0.05$). These findings suggest that VCP979 downregulated the degree of EMT in TGF-β1-stimulated HK-2 cells.

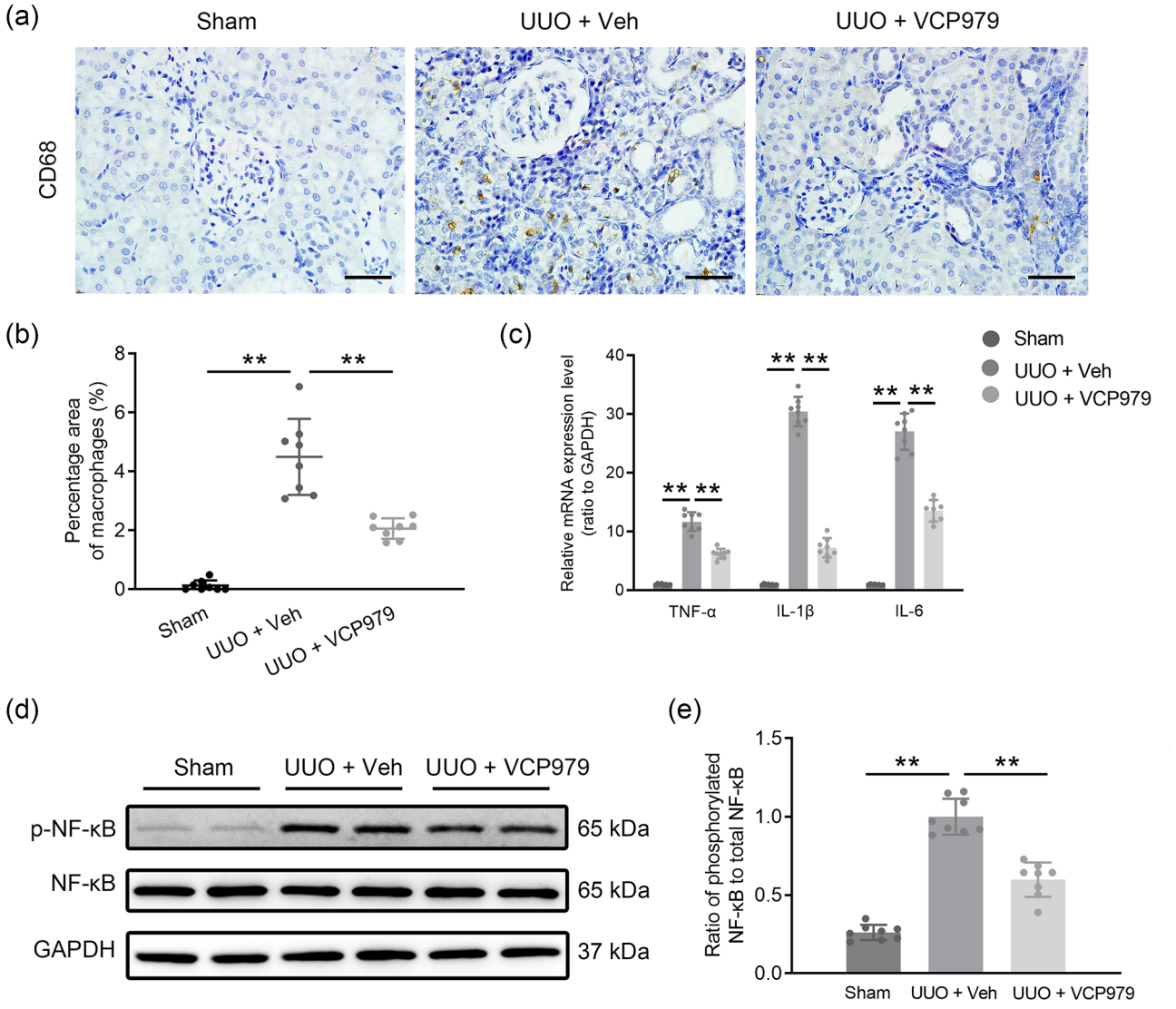

Figure 6. VCP979 reduced infiltration of macrophage and mitigated inflammatory level in UUO rats. (a) Immunochemical staining of CD68 and (b) quantitative assessment of percentage area of macrophages in kidney sections ($n=8$ per group; scale bars = 50 μm). (c) Relative mRNA expression of TNF-α, IL-1β, and IL-6 in kidney tissues ($n=8$ per group). (d) Western blot analysis and (e) quantitative assessment of the activation of NF-κB ($n=8$ per group). All data were presented as mean ± SD.
*$P<0.05$; **$P<0.01$.

VCP979 decreased the level of renal inflammation

IHC of CD68 was used to measure the infiltration of pro-inflammatory cells in renal tissues. As shown in Figure 6(a), the percentage area of infiltrated CD68 positive macrophages was significantly increased in the UUO + Veh group compared with the Sham group ($P<0.01$), which was significantly reduced in VCP979-treated UUO rats compared with the UUO + Veh group ($P<0.01$; Figure 6(b)). In addition, the mRNA levels of TNF-α, IL-1β, and IL-6 in renal tissues as detected by RT-qPCR were significantly decreased in the VCP979-treated UUO group compared with the UUO + Veh group ($P<0.01$; Figure 6(c)). Furthermore, the western blot analysis showed that the ratio of p-NF-κB/NF-κB was remarkably increased in the UUO + Veh group ($P<0.01$), and VCP979 significantly downregulated the ratio of p-NF-κB/NF-κB ($P<0.01$; Figure 6(d) and (e)). These data supported that VCP979 treatment could suppress the macrophages infiltration and the inflammatory cytokine gene expression in renal tissues.

VCP979 downregulated the expression of p38 MAPK, TGF-β1, and downstream Smad-dependent signaling pathways

To evaluate the efficacy of VCP979 on inhibiting the p38 MAPK, we employed the western blot analysis to measure the ratio of p-p38 MAPK/p38 MAPK in renal tissues. Western blot showed that VCP979-treated rats exhibited decreased ratio of p-p38 MAPK/p38 MAPK compared with the UUO + Veh rats ($P<0.01$; Figure 7(a) and (b)). The results confirmed that treatment with VCP979 inhibited the activation of p-p38 MAPK efficiently. Moreover, VCP979 treatment notably suppressed the expression of TGF-β1 in UUO rats compared with the UUO + Veh rats ($P<0.01$; Figure 7(a) and (c)). To further explore the underlying antifibrotic

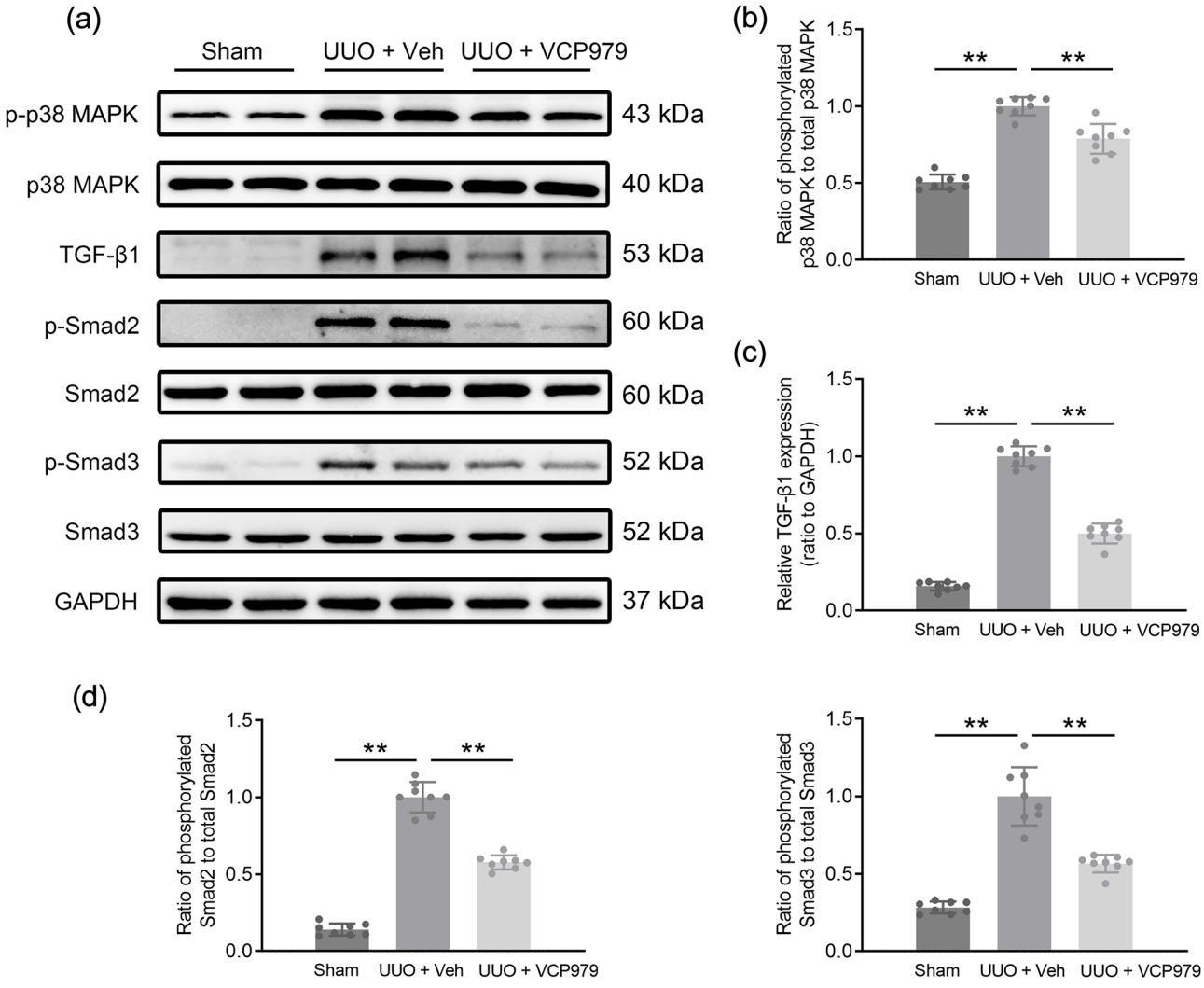

Figure 7. VCP979 suppress the expression of p-p38/p38 MAPK, TGF-β1 and inhibited downstream Smad-dependent signaling pathway in UUO rats. (a) Western blot of the protein expression level of p-p38 MAPK, p38 MAPK, TGF-β1, p-Smad2, Smad2, p-Smad3, and Smad3 ($n = 8$ per group). (b) Measured ratio of p-p38 MAPK to p38 MAPK protein expression of the three groups. (c) Measured protein expression of TGF-β1 in the three groups. (d) Measured ratio of p-Smad2/Smad2 and p-Smad3/Smad3 protein expression of the three groups. All data were shown as mean ± SD.
*$P < 0.05$; **$P < 0.01$.

mechanism of VCP979, we evaluated the effect of VCP979 on TGF-β1-induced activation of canonical Smad-dependent pathway. As shown in Figure 7(a) and (d), treatment with VCP979 significantly reduced the ratio of p-Smad2/Smad2 and p-Smad3/Smad3 ($P < 0.01$). These data supported that VCP979 could suppress TGF-β1-activated Smad-dependent signaling pathways.

Toxicity of VCP979

The toxicity of VCP979 was indicated by CCK-8 *in vitro* and liver function (AST and ALT) and H&E staining of liver in animal models. Cell viability was not affected by VCP979 as measured by CCK-8 assay (Figure 8(a)). In addition, no significant difference was observed in body weight between the three groups (Figure 8(b)). Moreover, the levels of AST and ALT in serum were assessed, and no difference was observed between three groups (Figure 8(c)). Results of H&E staining confirmed that there was no evident impact on the pathology of liver induced by administration of VCP979 (Figure 8(d)).

Discussion

Renal fibrosis is a chronic process featured by deregulated wound healing, uncontrolled inflammatory response, and excessive ECM deposition in the interstitial space of the kidney.[32] Although renal fibrosis is fatal and drives the progression of chronic kidney disease, there is still a lack of effective treatment for renal fibrosis.[33] VCP979 is a small-molecule compound that we have recently developed at the Monash University as a novel antifibrotic and anti-inflammatory agent.[13–15] In this study, we provided the first evidence of VCP979 application in renal fibrosis, and demonstrated that administration of VCP979 could alleviate renal fibrosis and inflammation in a rat model of UUO through *in vivo* MRI and *ex vivo* pathological analysis.

Renal fibrosis is a major public health issue with around 10% of the adult population at risk and is recognized as the final common pathway for all kidney diseases.[34,35] The p38 MAPK pathway is a potential regulator of the inflammatory and fibrotic process, and multiple therapeutic strategies have

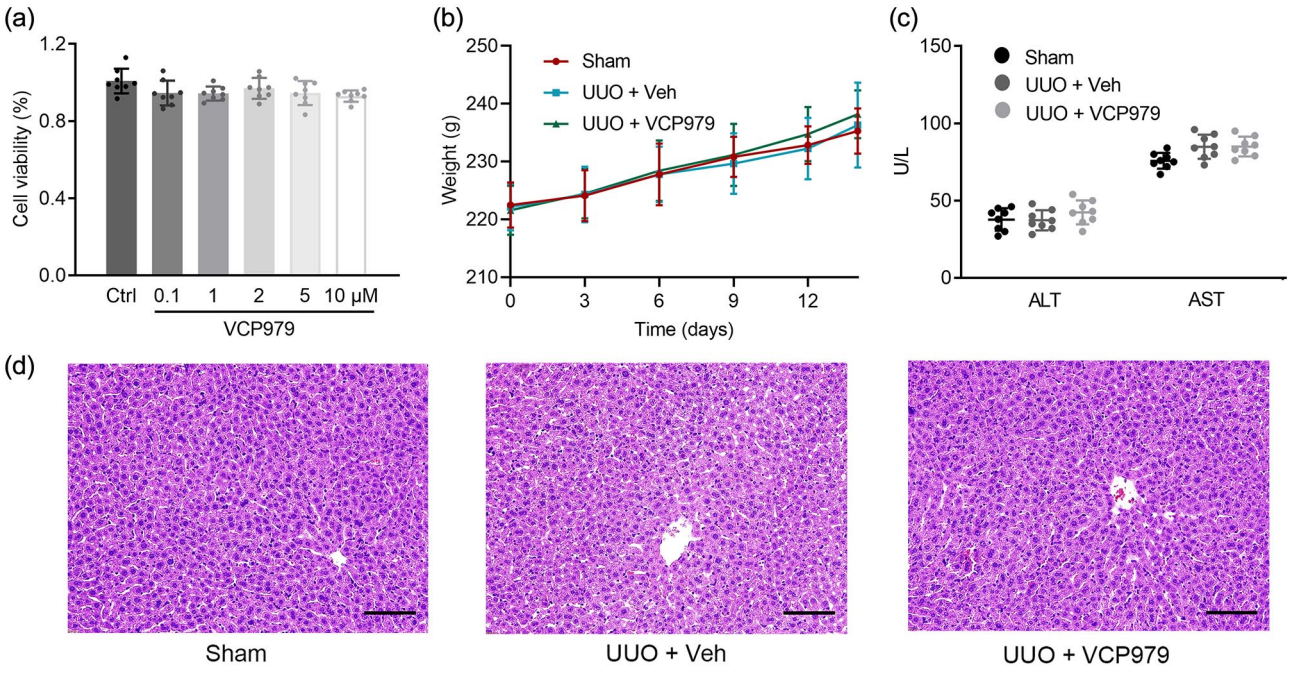

Figure 8. Safety of VCP979 treatment in HK-2 cells and rats. (a) The relative cell viability of HK-2 cells after incubation with various concentrations of VCP979 ($n = 8$ per group). (b) The body weight of rats in three groups was recorded once per three days after surgery ($n = 8$ per group). (c) The AST and ALT levels in serum were measured in three groups ($n = 8$ per group). (d) H&E-stained histological sections of the liver of rats after 14 days ($n = 8$ per group; scale bars = 100 μm). All data were presented as mean ± SD.
AST: alanine aminotransferase; ALT: aspartate aminotransferase; H&E: hematoxylin and eosin.

been exploited to impede the p38 MAPK pathway.[5,6] p38 MAPK inhibitors has been administration to mitigate tubular interstitial fibrosis in animal models of kidney disease, and inhibiting p38 MAPK has also been explored as a therapeutic strategy in a variety of clinical trials.[36–39] However, the classic p38 MAPK inhibitor SB203580 has an unsatisfactory *in vivo* activity.[15] Besides, the clinical p38 MAPK inhibition with losmapimod in a Phase II trial did not result in more than 50% reduction of proteinuria in patients with idiopathic focal segmental glomerulosclerosis,[36] and a p38 MAPK inhibitor LY3007113 was not planned for further clinical development as toxicity precluded achieving a biologically effective dose in a Phase I clinical trial.[38] Thus, novel p38 MAPK inhibitors with high potency and safety are urgently needed.

The p38 MAPK inhibitors are isoform-selective, and a series of novel p38 MAPK inhibitors with high selectivity for the p38α isoform over the other isoforms such as the p38β isoform has been identified. p38 MAPK is implicated in the intracellular responses to renal inflammation and fibrosis, but the currently available p38 MAPK inhibitors, such as SB203580, inhibit both the p38α and p38β MAPK isoforms and present low specificity, resulting in low potency and high toxicity.[15] Previous animal studies have demonstrated that inhibition of a single p38α isoform is responsible for an anti-inflammatory effect and inhibition of the p38β isoform alone showed no effect on the modulation of inflammatory TNF-α levels.[40] An inhibitor of p38 MAPK with a potent affinity for the active form of p38α MAPK is likely to have less toxic effect,[12] and may play a promising role in regulating the fibrotic signaling transduction in renal diseases. Herein, we developed a novel MAPK inhibitor, VCP979 which is a small-molecule compound and selective p38 MAPKα inhibitor, and it is a much poor inhibitor of p38 MAPKβ and does not inhibit the p38 MAPKγ or δ isoform. The advantages of VCP979 over other p38 MAPK inhibitors such as RWJ67657, a selective inhibitor of p38α and p38β, have been demonstrated by our previous studies.[15]

We utilized VCP979 to investigate its role in renal fibrosis. The renal pathological staining of Masson and Sirius red showed decreased percentage of fibrotic area after treatment with VCP979 for one week, and fibronectin staining demonstrated significantly decreased ECM accumulation in renal tissues. Since myofibroblasts are derived from renal fibroblasts and EMT of resident tubular epithelial cells,[41] the IHC and western blot results showed that administration of VCP979 decreased the expression of α-SMA and Vimentin, and increased the expression of E-cadherin, confirming that VCP979 relieved ECM accumulation and EMT process. To further explore the underlying antifibrotic mechanism of VCP979, we evaluated the effect of VCP979 on TGF-β1 signaling and TGF-β1-induced activation of canonical Smad-dependent pathway, and the results revealed that TGF-β1 was downregulated by VCP979 in obstructed kidney. Treatment with VCP979 also inhibited the activation of Smad2/Smad3, indicating that VCP979 could ameliorate renal fibrosis via the reduction of TGF-β1/Smads signaling pathways.

p38 MAPK pathway is also well-recognized to play an important role in the production of pro-inflammatory mediators and exert pro-inflammatory effects.[42] It is established that inflammation plays an essential role in the development of renal fibrosis, and persistent inflammation induced by chronic injury could advance fibrogenesis and further tissue damage. The association between fibrogenesis and the inflammatory response has been established and confirmed by morphological evidence.[43] Thus, in this study, IHC of CD68 was used to measure the infiltration

of macrophages in renal tissue, which demonstrated that VCP979 mitigated the recruitment of macrophage. In addition, RT-qPCR showed that VCP979 decreased the mRNA expression of TNF-α, IL-1β, and IL-6. Besides, previous studies have reported that phosphorylation of NF-κB promotes the activation of fibroblast and renal fibrosis directly,[44] and tubular EMT was induced by direct contact between tubular and monocyte cells *via* an NF-κB-dependent pathway.[45] Thus, this study also investigated the NF-κB through western blot analysis and showed that the NF-κB pathway was inhibited after treatment with VCP979. These results revealed that VCP979 could attenuate the expression of inflammatory cytokines and inhibit the NF-κB pathway in renal tissues effectively.

Increasing evidences suggest that T1rho mapping can be used to quantify the macromolecular environment *in vivo*, and ECM deposition is associated with an elevation of T1rho values.[19–21] For example, Hu *et al*.[46] have reported that the T1rho values were correlated with the progression of renal fibrogenesis after UUO in a rat model, which indicated that T1rho is a candidate biomarker of renal fibrosis. Since T1rho mapping gives information about ECM deposition and permits measurement of renal fibrosis, here we have used T1rho mapping to visualize the fibrotic burden of kidney after UUO. Our results verified that the T1rho values were decreased after treatment with VCP979 in renal tissues of UUO rats, and a positive correlation was observed between the T1rho value and the percentage of fibrotic area, confirming the feasibility of applying T1rho mapping to quantify the alterations of renal fibrosis after treatment with VCP979 in murine models of UUO *in vivo*.

There are a few limitations in this study. First, the effects of VCP979 treatment on renal ECM deposition were detected by the expression of fibronectin in UUO kidneys by IHC, while ECM deposition includes several indicators such as collagen I and IV. In addition, no control group was established to assess the difference between the commercial p38 MAPK inhibitors such as inhibitors against both p38α and p38β and the VCP979 treatment group, but the advantages of VCP979 over other p38 MAPK inhibitors such as RWJ67657, a selective inhibitor of p38α and p38β, have been demonstrated by our previous studies. Our follow-up studies will further seek better understanding of the effects of VCP979 on renal fibrosis by tracking the medication and functional changes of different selective inhibitors through systematical investigations to fully display the advantages and side effects of VCP979 *in vitro* and *in vivo*. Furthermore, according to epidemiology and outcomes of chronic renal disease, sex hormones have been implicated in modulating inflammation, oxidative stress, and fibrosis in renal structural remodeling. Therefore, it is necessary to consider gender-specific differences in the design of experimental research and further investigate the effects of gender and sex hormones on renal fibrosis using both male and female UUO rats.

To our knowledge, this study was the first to validate VCP979, a novel small-molecule compound, may attenuate renal fibrosis in UUO rats through anti-inflammatory and antifibrotic effects, and the capability of T1rho MRI to detect the alteration of renal tissue fibrosis after VCP treatment makes it a potential imaging approach to visualize renal fibrosis non-invasively. The protective effects of VCP979 in the UUO rat model were attributed to the attenuation of inflammatory-fibrotic response and suppression of the p38 MAPK signaling pathway. Since p38 MAPK inhibitors have been extensively evaluated in animal study and clinical trials, these findings may facilitate the application of novel small-molecule compound p38 inhibitors with better *in vivo* anti-inflammatory and antifibrotic activities in different kidney diseases associated with fibrosis.

AUTHORS' CONTRIBUTIONS

SM and DC conceptualized the problem. SM, DC, Y-CW, and T-TX conceptualized the problem. SM, DC, and JZ developed an experimental method. SM, DC, and HG conducted the experiments. DC, HG, and BW did the literature research. SM and DC wrote the manuscript. SM, DC, HG, and SJ collected the resources. DC, HG, and SJ reviewed and edited the manuscript. BW and SJ supervised the manuscript.

DECLARATION OF CONFLICTING INTERESTS

The author(s) declared no potential conflicts of interest with respect to the research, authorship, and/or publication of this article.

FUNDING

The author(s) disclosed receipt of the following financial support for the research, authorship, and/or publication of this article: This work was supported by the National Natural Science Foundation of China (NSFC, nos 81830053, 81801759, 92059202, and 61821002), the Science Foundation for Creative Research Groups of the Ministry of Science and Technology of China (no. 6290002012), the Key Research and Development Program of Jiangsu Province (BE2020717), and the Natural Science Foundation of Jiangsu Province (BK20180375).

ORCID ID

Shenghong Ju https://orcid.org/0000-0001-5041-7865

SUPPLEMENTAL MATERIAL

Supplemental material for this article is available online.

REFERENCES

1. Nastase MV, Zeng-Brouwers J, Wygrecka M, Schaefer L. Targeting renal fibrosis: mechanisms and drug delivery systems. *Adv Drug Deliv Rev* 2018;**129**:295–307
2. Webster AC, Nagler EV, Morton RL, Masson P. Chronic kidney disease. *Lancet* 2017;**389**:1238–52
3. Kuppe C, Ibrahim MM, Kranz J, Zhang X, Ziegler S, Perales-Patón J, Jansen J, Reimer KC, Smith JR, Dobie R, Wilson-Kanamori JR, Halder M, Xu Y, Kabgani N, Kaesler N, Klaus M, Gernhold L, Puelles VG, Huber TB, Boor P, Menzel S, Hoogenboezem RM, Bindels EMJ, Steffens J, Floege J, Schneider RK, Saez-Rodriguez J, Henderson NC, Kramann R. Decoding myofibroblast origins in human kidney fibrosis. *Nature* 2021;**589**:281–6
4. Arkin MR, Wells JA. Small-molecule inhibitors of protein-protein interactions: progressing towards the dream. *Nat Rev Drug Discov* 2004;**3**:301–17
5. Stambe C, Atkins RC, Tesch GH, Masaki T, Schreiner GF, Nikolic-Paterson DJ. The role of p38alpha mitogen-activated protein kinase activation in renal fibrosis. *J Am Soc Nephrol* 2004;**15**:370–9
6. Furukawa F, Matsuzaki K, Mori S, Tahashi Y, Yoshida K, Sugano Y, Yamagata H, Matsushita M, Seki T, Inagaki Y, Nishizawa M, Fujisawa J, Inoue K. P38 MAPK mediates fibrogenic signal through Smad3 phosphorylation in rat myofibroblasts. *Hepatology* 2003;**38**:879–89

7. Denhez B, Rousseau M, Dancosst DA, Lizotte F, Guay A, Auger-Messier M, Côté AM, Geraldes P. Diabetes-induced DUSP4 reduction promotes podocyte dysfunction and progression of diabetic nephropathy. *Diabetes* 2019;**68**:1026–39
8. Wang D, Warner GM, Yin P, Knudsen BE, Cheng J, Butters KA, Lien KR, Gray CE, Garovic VD, Lerman LO, Textor SC, Nath KA, Simari RD, Grande JP. Inhibition of p38 MAPK attenuates renal atrophy and fibrosis in a murine renal artery stenosis model. *Am J Physiol Renal Physiol* 2013;**304**:F938–47
9. Meng XM, Nikolic-Paterson DJ, Lan HY. TGF-beta: the master regulator of fibrosis. *Nat Rev Nephrol* 2016;**12**:325–38
10. Zhao X, Kwan JYY, Yip K, Liu PP, Liu FF. Targeting metabolic dysregulation for fibrosis therapy. *Nat Rev Drug Discov* 2020;**19**:57–75
11. Gu YY, Liu XS, Huang XR, Yu XQ, Lan HY. TGF-β in renal fibrosis: triumphs and challenges. *Future Med Chem* 2020;**12**:853–66
12. Shah NG, Tulapurkar ME, Ramarathnam A, Brophy A, Martinez R III, Hom K, Hodges T, Samadani R, Singh IS, MacKerell AD, Shapiro P, Hasday JD. Novel noncatalytic substrate-selective p38alpha-specific MAPK inhibitors with endothelial-stabilizing and anti-inflammatory activity. *J Immunol* 2017;**198**:3296–306
13. Liu J, Meng Q, Liang X, Zhuang R, Yuan D, Ge X, Cao H, Lin F, Gong X, Fan H, Wang B, Zhou X, Liu Z. A novel small molecule compound VCP979 improves ventricular remodeling in murine models of myocardial ischemia/reperfusion injury. *Int J Mol Med* 2020;**45**:353–64
14. Xu T, Ding J, Ge H, Xu X, Scammells P, Wang B, Ju S. Effects of VCP979 novel p38 mitogen activated protein kinase inhibitor on progression of pancreatic cancer in mouse model with diabetic conditions. *J Biomed Nanotechnol* 2019;**15**:1325–33
15. Cai Y, Lu C, Xu T, Ma Y, Min S, Scammells P, Wang B, Ju S. Diffusion tensor imaging evaluation of axonal/white matter remodeling in a mouse model of diabetic stroke treated with novel p38 MAPK inhibitor, VCP979. *J Biomed Nanotechnol* 2018;**14**:585–93
16. Jiang K, Ferguson CM, Lerman LO. Noninvasive assessment of renal fibrosis by magnetic resonance imaging and ultrasound techniques. *Transl Res* 2019;**209**:105–20
17. Whittier WL, Korbet SM. Timing of complications in percutaneous renal biopsy. *J Am Soc Nephrol* 2004;**15**:142–7
18. Capretz T, Patel RM, Okhunov Z. Percutaneous renal biopsy: approach, diagnostic accuracy and risks. *Curr Opin Urol* 2018;**28**:369–74
19. Hu G, Liang W, Wu M, Lai C, Mei Y, Li Y, Xu J, Luo L, Quan X. Comparison of T1 mapping and T1rho values with conventional diffusion-weighted imaging to assess fibrosis in a rat model of unilateral ureteral obstruction. *Acad Radiol* 2019;**26**:22–9
20. Thompson EW, Kamesh Iyer S, Solomon MP, Li Z, Zhang Q, Piechnik S, Werys K, Swago S, Moon BF, Rodgers ZB, Hall A, Kumar R, Reza N, Kim J, Jamil A, Desjardins B, Litt H, Owens A, Witschey WRT, Han Y. Endogenous T1ρ cardiovascular magnetic resonance in hypertrophic cardiomyopathy. *J Cardiovasc Magn Reson* 2021;**23**:120
21. Morrell GR, Zhang JL, Lee VS. Magnetic resonance imaging of the fibrotic kidney. *J Am Soc Nephrol* 2017;**28**:2564–70
22. Zou L, Jiang J, Zhang H, Zhong W, Xiao M, Xin S, Wang Y, Xing W. Comparing and combining MRE, T1ρ, SWI, IVIM, and DCE-MRI for the staging of liver fibrosis in rabbits: assessment of a predictive model based on multiparametric MRI. *Magn Reson Med* 2022;**87**:2424–35
23. van Oorschot JW, Guclu F, de Jong S, Chamuleau SA, Luijten PR, Leiner T, Zwanenburg JJ. Endogenous assessment of diffuse myocardial fibrosis in patients with T1rho-mapping. *J Magn Reson Imaging* 2017;**45**:132–8
24. Hectors SJ, Bane O, Kennedy P, El Salem F, Menon M, Segall M, Khaim R, Delaney V, Lewis S, Taouli B. T1ρ mapping for assessment of renal allograft fibrosis. *J Magn Reson Imaging* 2019;**50**:1085–91
25. Wang F, Otsuka T, Takahashi K, Narui C, Colvin DC, Harris RC, Takahashi T, Gore JC. Renal tubular dilation and fibrosis after unilateral ureter obstruction revealed by relaxometry and spin-lock exchange MRI. *NMR Biomed* 2021;**34**:e4539
26. Percie du Sert N, Hurst V, Ahluwalia A, Alam S, Avey MT, Baker M, Browne WJ, Clark A, Cuthill IC, Dirnagl U, Emerson M, Garner P, Holgate ST, Howells DW, Karp NA, Lazic SE, Lidster K, MacCallum CJ, Macleod M, Pearl EJ, Petersen OH, Rawle F, Reynolds P, Rooney K, Sena ES, Silberberg SD, Steckler T. The ARRIVE guidelines 2.0: updated guidelines for reporting animal research. *BMJ Open Sci* 2020;**4**:e100115
27. Oka M, Sekiya S, Sakiyama R, Shimizu T, Nitta K. Hepatocyte growth factor-secreting mesothelial cell sheets suppress progressive fibrosis in a rat model of CKD. *J Am Soc Nephrol* 2019;**30**:261–76
28. Chang D, Wang YC, Xu TT, Peng XG, Cai Y, Wang L, Bai YY, Ju S. Noninvasive identification of renal hypoxia in experimental myocardial infarctions of different sizes by using BOLD MR imaging in a mouse model. *Radiology* 2018;**286**:129–39
29. Chang X, Zhen X, Liu J, Ren X, Hu Z, Zhou Z, Zhu F, Ding K, Nie J. The antihelmenthic phosphate niclosamide impedes renal fibrosis by inhibiting homeodomain-interacting protein kinase 2 expression. *Kidney Int* 2017;**92**:612–24
30. Li R, Guo Y, Zhang Y, Zhang X, Zhu L, Yan T. Salidroside ameliorates renal interstitial fibrosis by inhibiting the TLR4/NF-kappaB and MAPK signaling pathways. *Int J Mol Sci* 2019;**20**:1103
31. Chung AC, Zhang H, Kong YZ, Tan JJ, Huang XR, Kopp JB, Lan HY. Advanced glycation end-products induce tubular CTGF via TGF-beta-independent Smad3 signaling. *J Am Soc Nephrol* 2010;**21**:249–60
32. Djudjaj S, Boor P. Cellular and molecular mechanisms of kidney fibrosis. *Mol Aspects Med* 2019;**65**:16–36
33. Breyer MD, Susztak K. The next generation of therapeutics for chronic kidney disease. *Nat Rev Drug Discov* 2016;**15**:568–88
34. Li X, Pan J, Li H, Li G, Liu X, Liu B, He Z, Peng Z, Zhang H, Li Y, Xiang X, Chai X, Yuan Y, Zheng P, Liu F, Zhang D. DsbA-L mediated renal tubulointerstitial fibrosis in UUO mice. *Nat Commun* 2020;**11**:4467
35. Rayego-Mateos S, Valdivielso JM. New therapeutic targets in chronic kidney disease progression and renal fibrosis. *Expert Opin Ther Targets* 2020;**24**:655–70
36. Gipson DS, Hladunewich MA, Lafayette R, Sedor JR, Rovin BH, Barbour SJ, McMahon A, Jennette JC, Nachman PH, Willette RN, Paglione M, Gao F, Ross Terres JA, Vallow S, Holland MC, Thorneloe KS, Sprecher DL. Assessing the impact of losmapimod on proteinuria in idiopathic focal segmental glomerulosclerosis. *Kidney Int Rep* 2020;**5**:1228–39
37. O'Donoghue ML, Glaser R, Aylward PE, Cavender MA, Crisp A, Fox KA, Laws I, Lopez-Sendon JL, Steg PG, Theroux P, Sabatine MS, Morrow DA. Rationale and design of the losmapimod to inhibit p38 MAP kinase as a therapeutic target and modify outcomes after an acute coronary syndrome trial. *Am Heart J* 2015;**169**:622–30.e6
38. Goldman JW, Rosen LS, Tolcher AW, Papadopoulos K, Beeram M, Shi P, Pitou C, Bell R, Kulanthaivel P, Zhang X, Fink A, Chan EM, Shahir A, Farrington D, Patnaik A. Phase 1 and pharmacokinetic study of LY3007113, a p38 MAPK inhibitor, in patients with advanced cancer. *Invest New Drugs* 2018;**36**:629–37
39. Zhou J, Zhong J, Huang Z, Liao M, Lin S, Chen J, Chen H. TAK1 mediates apoptosis via p38 involve in ischemia-induced renal fibrosis. *Artif Cells Nanomed Biotechnol* 2018;**46**:1016–25
40. O'Keefe SJ, Mudgett JS, Cupo S, Parsons JN, Chartrain NA, Fitzgerald C, Chen SL, Lowitz K, Rasa C, Visco D, Luell S, Carballo-Jane E, Owens K, Zaller DM. Chemical genetics define the roles of p38alpha and p38beta in acute and chronic inflammation. *J Biol Chem* 2007;**282**:34663–71
41. Guo Y, Xiao Y, Zhu H, Guo H, Zhou Y, Shentu Y, Zheng C, Chen C, Bai Y. Inhibition of proliferation-linked signaling cascades with atractylenolide I reduces myofibroblastic phenotype and renal fibrosis. *Biochem Pharmacol* 2021;**183**:114344
42. Amos LA, Ma FY, Tesch GH, Liles JT, Breckenridge DG, Nikolic-Paterson DJ, Han Y. ASK1 inhibitor treatment suppresses p38/JNK signalling with reduced kidney inflammation and fibrosis in rat crescentic glomerulonephritis. *J Cell Mol Med* 2018;**22**:4522–33
43. Mack M. Inflammation and fibrosis. *Matrix Biol* 2018;68–9:106–21
44. Liao Y, Tan RZ, Li JC, Liu TT, Zhong X, Yan Y, Yang JK, Lin X, Fan JM, Wang L. Isoliquiritigenin attenuates UUO-induced renal inflammation and fibrosis by inhibiting Mincle/Syk/NF-Kappa B signaling pathway. *Drug Des Devel Ther* 2020;**14**:1455–68
45. Li Q, Liu BC, Lv LL, Ma KL, Zhang XL, Phillips AO. Monocytes induce proximal tubular epithelial-mesenchymal transition through NF-kappa B dependent upregulation of ICAM-1. *J Cell Biochem* 2011;**112**:1585–92
46. Hu G, Liang W, Wu M, Lai C, Mei Y, Li Y, Xu J, Luo L, Quan X. Comparison of T1 mapping and T1ρ values with conventional diffusion-weighted imaging to assess fibrosis in a rat model of unilateral ureteral obstruction. *Acad Radiol* 2019;**26**:22–9

(Received June 12, 2022, Accepted November 4, 2022)